J Nanopart Res (2015) 17:305
DOI 10.1007/s11051-015-3097-z

RESEARCH PAPER

Preparation of thermo and pH-responsive polymer@Au/Fe_3O_4 core/shell nanoparticles as a carrier for delivery of anticancer agent

Marjan Ghorbani · Hamed Hamishehkar · Naser Arsalani · Ali Akbar Entezami

Received: 25 March 2015 / Accepted: 27 June 2015 / Published online: 12 July 2015

Abstract In this work, a thermo and pH-responsive poly-*N*-isopropylacrylamide-co-itaconic acid containing thiol side groups were successfully synthesized to prepare Doxorubicin-loaded polymer@Au/Fe_3O_4 core/shell nanoparticles (DOX-NPs). Copolymer and NPs were fully characterized by FT-IR, HNMR, photo-correlation spectroscopy, SEM, X-ray diffraction, vibrating-sample magnetometer, thermal gravimetric analysis, and UV–Vis spectroscopy. The stimuli-responsive characteristics of NPs were evaluated by in vitro release study in simulated cancerous environment. The biocompatibility and cytotoxic properties of NPs and DOX-NPs are explored by MTT method. The prepared NPs with the size of 50 nm showed paramagnetic characteristics with suitable and stable dispersion at physiological medium and high loading capacity (up to 55 %) of DOX. DOX-NPs yielded a pH- and temperature-triggered release of entrapped drugs at tumor tissue environment (59 % of DOX release) compared to physiological condition (20 % of DOX release) during 48 h. In vitro cytotoxicity studies indicated that the NPs showed no cytotoxicity on A549 cells at different amounts after incubation for 72 h confirming its suitability as a drug carrier. DOX-NPs, on the other hand, caused an efficient anticancer performance as verified by MTT assay test. It was concluded that developed NPs by us in this study may open the possibilities for targeted delivery of DOX to the cancerous tissues.

Keywords Dual stimuli-responsive · Core/shell · Au/Fe_3O_4 · Targeted drug delivery · Doxorubicin · Chemotherapy · Nanomedicine

M. Ghorbani · N. Arsalani · A. A. Entezami (✉)
Laboratory of Polymer, Faculty of Chemistry, University of Tabriz, Tabriz, Iran
e-mail: aentezami@tabrizu.ac.ir

H. Hamishehkar (✉)
Drug Applied Research Center, Tabriz University of Medical Sciences, Tabriz, Iran
e-mail: hamishehkarh@tbzmed.ac.ir

Introduction

Polymeric nanoparticles (NPs) have shown promising applications as nano-carriers of drugs and contrast agents due to their unique properties (Sahoo et al. 2013; Siegel 2014). Among the polymeric NPs, the nanomaterials with stimuli-responsive structure and function have attracted impressive interest among researchers in respect of delivery of various drugs, especially anticancer agents (Bawa et al. 2009; Salehi and Hamishehkar 2014; Sundaresan et al. 2014). Anticancer drugs can be conjugated to pH-sensitive polymers to take the benefit of the acidic environment of tumor. The existence of acid-sensitive spacers between the drug and polymer

assists the release of drug either in relatively acidic extracellular fluids or, after endocytosis in endosomes or lysosomes of tumor cells. Hence, it is anticipated that the pH-responsive drug-delivery systems will show a main role in applications in new horizons of cancer therapy (Zhu and Chen 2015). In addition, the temperature of tumor tissues have been reported to be a bit more than normal cells around 40 °C. Therefore, temperature sensitivity is one of the most interesting characteristics in stimulus-responsive polymeric nanocarriers and has been extensively applied for drug and gene delivery systems (Ganta et al. 2008). Thus, temperature and pH sensitivity are the major properties in stimuli-responsive polymers, which have been a topic of prevalent research (Nuopponen and Tenhu 2007; Du et al. 2009; Shi et al. 2014). It was proved that tumor tissue exhibits lower pH and higher temperature than that of normal tissues. These features can be applied for formulating the dual-sensitive carriers that smartly differentiate between normal and tumor tissues, achieving better targeting efficiency and treatment efficacy accompanying with reduction in associated side effects of anticancer drugs on normal tissues (Zhao et al. 2012; Liu et al. 2014). These polymers and copolymers place emphasis on the monomer *N*-isopropylacrylamide (NIPAAm) which has a low critical solution temperature (LCST) of 32 °C and can react with acrylic acid or other polymers to design new multifunctional materials. The drug release from these stimuli-responsive NPs much faster than rigid particles and can be controlled by changing of the outer environment (Liu et al. 2006; Bawa et al. 2009). Among these, nanomaterials hold great promise for a wide variety of applications, including in the biomedical field, as imaging tools (Lin et al. 2009; Yang et al. 2013), as phototherapy agents (Li et al. 2014a), or as drug carriers (Chao et al. 2010; Nigam et al. 2014). A great deal of attention has also been given to the preparation and application of colloidal gold and magnetic particles in recent years (Mahmoudi et al. 2011; Dykman and Khlebtsov 2012). In order to extend the applicability of Fe_3O_4 NPs, Au-coated Fe_3O_4 NPs have been fabricated to open wider possibilities of surface functionality and at the same time reduce surface oxidation (Lo et al. 2007; Tamer et al. 2009). Gold represents an excellent candidate by virtue of its easy reductive preparation, high chemical stability, and biocompatibility (Cui et al. 2005a, b; Liang et al. 2012). In these fields, the fine control of stability, particle size, and morphology of the NPs are important (Zhao et al. 2008). To improve their dispersibility, the core–shell of Au/Fe_3O_4 NPs may be coated with a protective stabilizer or with a water-soluble polymer (Liu et al. 2010; Chao et al. 2011; Shi et al. 2011; Salehizadeh et al. 2012). Most commonly, an ex situ approach is taken—a method based on the cooperative, preformed NPs in the presence of presynthesized stimuli-responsive polymers (Salmaso et al. 2009; Zhang et al. 2013; Hamner and Maye 2013). In general, polymers synthesized by reversible addition fragmentation chain transfer (RAFT) can produce polymer-protected gold NPs via ligand exchange by thiol end-groups or reduce gold salts in the presence of sulfur end-capped polymers (Zheng et al. 2006; Nuopponen and Tenhu 2007; Zhang et al. 2013; Li et al. 2014b). MC Cormick et al. reported that water-soluble polymers prepared by RAFT radical polymerization can stabilize gold NPs by reduction of dithioester end groups to thiol groups in the presence of $HAuCl_4$ (Lowe et al. 2002). Recently, the temperature behaviors of bulk and surface-grafted PNIPAAms were probed, and it was found that surface-bound polymer exhibited more gradual responses over a wide range of temperature (Yusa et al. 2007; Hamner and Maye 2013; Shi et al. 2014). For example, Hamner et al. reported that DNA-mediated assembly and encoded nanocarrier drug release could be regulated by thermoresponsive PNIPAAm-b-PMAA-protected AuNP (Hamner et al. 2013). In this study, we report the synthesis of a new type of the smart core/shell of Au/Fe_3O_4 NPs that is surface decorated by a dual stimuli-responsive copolymer of thiolated poly(*N*-isopropylacrylamide-co-Itaconic acid) (thiolated poly(NIPAAm-co-IA)) suitable for application as a carrier of anticancer agent. Despite common polymers which contain thiol end group prepared by RAFT agents, this polymeric shell includes thiol side groups in the backbone of the copolymer. To our knowledge, there is no report of the synthesis of the proposed structure and its application for delivery of doxorubicin (DOX), a well-known potent anticancer agent.

Experimental section

Materials

Ferrous chloride tetrahydrate ($FeCl_2$, $4H_2O$), ferric chloride hexahydrate ($FeCl_3$, $6H_2O$), sodium citrate dehydrate, ammonia solution (25–28 %), carbonyldiimidazole (CDI), perchloric acid ($HClO_4$, 70–72 %), and 2-aminoethanethiol (AET) were purchased from Merck. Hydrogen tetrachloroaurate (III) trihydrate ($HAuCl_4$), Itaconic acid (IA), dipyridyl disulfide (DPDS), dimethylsulfoxide (DMSO), tetrahydrofuran (THF), and dithiothreitol (DTT) were purchased from Sigma-Aldrich. *N*-Isopropylacrylamide (NIPAAm, 99 %) was purchased from Acros. DOX was kindly donated by Exir Nano Sina Company (Iran). DMSO was totally dried and then distilled under reduced pressure. THF was dried and distilled after refluxing for 3 h. Double-distilled water was used for all experiments.

S-(2-Pyridylthio)cysteamine Hydrochloride(AE–S–S–Py)

S-(2-Pyridylthio)cysteamine Hydrochloride was synthesized according to the reported literature procedures (Ebright et al. 1992). Pyridyl disulfide (2.2 g, 10 mmol) was dissolved in 0.8 mL of acetic acid and 20 mL of methanol. Into this solution was added dropwise 2-aminoethanethiol hydrochloride (0.57 g, 5 mmol, 10 mL methanol) over a period of 0.5 h. The reaction mixture was stirred for an additional 48 h and was then evaporated under high vacuum to obtain yellow oil. The product was washed with 50 mL of diethyl ether and then was dissolved in 10 mL of methanol. Finally, the product was precipitated by addition of 50 mL of diethyl ether and was redissolved in 10 mL of methanol (three times).

Synthesis of poly(NIPAAm-co-IA)

The copolymerization of the NIPAAm with IA was carried out in DMSO at 70 °C with AIBN as radical initiator with mole ratio of [NIPAAM]/[IA]/[AIBN] 85:15:100. In a typical polymerization, in order to prepare poly(NIPAAm-co-IA), NIPAAm (2 g, 17.7 mmol), itaconic acid (0.4 g, 3.1 mmol), and AIBN (0.034 g, 0.2 mmol) were dissolved in DMSO. The reaction system was degassed by bubbling with nitrogen for 30 min. Then, the polymerization reaction was performed at 70 °C under nitrogen atmosphere with continuous mechanical stirring for 24 h. The polymer solution was precipitated in an excess diethyl ether, filtered, and finally vacuum-dried.

Synthesis of poly(NIPAAm-co-IA) containing thiol side groups (polymer)

Copolymer of poly(NIPAAm-co-IA) (0.5 g) was dissolved in dry DMSO (8 mL). CDI (365 mg, 2.25 mmol) was added into the polymer solution under argon atmosphere at room temperature. Then, the mixture was stirred under argon for another 3 h at room temperature. 2-(2-Pyridyldithio)ethylamine hydrochloride (100.2 mg, 0.45 mmol) followed by triethylamine (63 μL, 0.45 mmol) was added to the reaction solution under argon atmosphere, and stirring was continued overnight. Afterward, 2 mL of concentrated aqueous NH_3 was added, and the mixture was stirred for 45 min. The obtained material in DMSO was treated with DTT (694 mg, 4.5 mmol) under exclusion of oxygen which led to degradation –S–S–Py-appended groups within 10 min. Clear DMSO solution was stirred with DTT under argon for 48 h more. The final synthesized polymer solution was diluted with HCl (pH = 3) and transferred to 1000 Mw cutoff dialysis tubing. Dialysis was performed twice against diluted HCl (pH = 3).

Synthesis of Fe_3O_4 NPs

Iron oxide (Fe_3O_4) NPs were synthesized according to the literature procedure (Massart 1981). In brief, 4 mL ferric chloride solution (1 M) and 1 mL ferrous chloride solution (2 M, in HCl 2 N) were mixed and added into 50 mL ammonia solution (0.7 M). After stirring the reaction mixture for 30 min, the precipitate was isolated by magnetic decantation and stirred with 50 mL diluted $HClO_4$ (2 M). Then, the resulting colloidal suspension was isolated by centrifugation, and the residue was diluted to make up 50 mL with water.

Synthesis of Au/Fe_3O_4 NPs

The synthesis of Au/Fe_3O_4 NPs was carried out according to Choi et al. (Lo et al. 2007). In order to obtain the core/shell of Au/Fe_3O_4 NPs, 15 mL

$HAuCl_4$ (2 mg/mL) solution was added into 100 mL of water and then heated to boiling. At this point, 5 mL of presynthesized Fe_3O_4 NPs was poured into the reaction flask followed by the addition of 5 mL sodium citrate (80 mM) under stirring. The color of the solution changed from brown to wine red under stirring for 5 min.

Preparation of smart polymer@Au/Fe_3O_4 core/shell NPs

A total volume of 30 mL of citrate-stabilized Au/Fe_3O_4 NPs solution was mixed with 60 mg of polymer and kept under stirring overnight at room temperature. The resulting conjugates were purified by a permanent magnet to remove the excess polymer followed by redispersion in pure water.

Determination of the thiol group content

The quantity of thiol groups on the polymer was characterized by iodometric titration (Kast and Bernkop-Schnürch 2002). At first, 10 mg of polymer was dissolved in 3 mL of DI water. Then, the pH value was adjusted to pH = 3 by addition of HCl (1 N). Afterward, 300 μL of aqueous starch solution (1 %) was added, and the solution was titrated with an aqueous iodin solution (1 mM) until constant light blue color was maintained. The concentration of the thiol groups in polymer was calculated to be 0.063 mmol/g.

Loading of drug in polymer@Au/Fe_3O_4 NPs

The drug loading of the resultant polymer@Au/Fe_3O_4 NPs was investigated using DOX as a model molecule. The procedure is described as follows: 500 μL DOX solution (10 mg/mL) was added into 1 mL polymer@Au/Fe_3O_4 NPs (5 mg/mL) suspension. Then, the mixture was incubated in a shaker for 24 h at room temperature to prepare DOX-loaded polymer@Au/Fe_3O_4 NPs (DOX-NPs). The unloaded drug was separated from the DOX-NPs by means of an external magnet and then its concentration determined by HPLC method. The mobile phase consisted of a mixture (45:55) of acetonitrile:potassium dihydrogen phosphate aqueous solution (10 mM) at pH = 3 at a flow rate of 1 mL/min, with UV detection at 254 nm. The encapsulation efficiency (EE) and loading capacity (LC) percentages were calculated according to the following equations:

$$\text{Encapsulation efficiency } (\%, \text{w/w}) = \frac{\text{Mass of drug in nanoparticles}}{\text{Mass of initial added drug}} \times 100$$

$$\text{Loading capacity } (\%, \text{w/w}) = \frac{\text{Mass of drug in nanoparticles}}{\text{Mass of nanoparticles}} \times 100$$

In vitro release of DOX

1 mL of DOX-NPs suspension (5 mg/mL) were introduced into dialysis bags (molecular weight cut off 12 kDa, Sigma-Aldrich, USA) and then immersed into 15 mL of phosphate buffered saline (PBS) in both physiologic (pH 7.4, 37 °C) and simulated cancerous tissue (pH 5.3, 40 °C) conditions. Furthermore, DOX-NPs were incubated in pH 7.4, 40 °C and pH 5.3, 37 °C to assess the pH and temperature responsive ability of prepared polymer@Au/Fe_3O_4 NPs accurately. At predetermined intervals, 200 μL of the solution was taken out periodically from the reservoir and drug concentration was analyzed using HPLC instrument. For keeping a constant volume, 200 μL of the fresh buffer medium was added back to the reservoir after each sampling.

In vitro cell assays

The biocompatibility of the polymer@Au/Fe_3O_4 and DOX-NPs was measured by MTT assay. Human lung carcinoma A549 line was purchased from NCBI (National Cell Bank of Iran, Pasteur Institute) as the target cells and was used to evaluate the cytotoxicity of the NPs. A549 cell line were maintained in RPMI1640 with 10 % fetal bovine serum (FBS) at 37 °C in 5 % CO_2 and 95 % air with more than 95 % humidity. The cells were seeded into a 96-well plate at 1×10^4 cells/well. After incubation for 24 h (37 °C, 5 % CO_2), the culture medium was removed, and 200 μL growth mediums containing various concentrations of DOX-free polymer@Au/Fe_3O_4 NPs, and DOX-NPs was added to each well and incubated for 72 h. After finishing incubation, the medium containing NPs was exchanged with a 150 μL of fresh medium, and 50 μL aliquots of MTT solution (5 mg/mL) for further 4-h incubation. Then, the growth

medium and excess MTT were removed, and DMSO (200 μL) was added to each well to dissolve the purple formazan crystals. The optical density (OD) values were measured at 570 nm with a background correction at 630 nm using a microplate reader, and the cell viability was calculated from the following equation:

$$\text{Cell viability}\,(\%) = \frac{\text{OD sample}}{\text{OD control}} \times 100\,\%$$

Characterization

^{1}H-NMR spectrum was recorded at 25 °C on a 400 MHz NMR spectrometer (Bruker, Germany). The Sample was dissolved in $CDCl_3$ at room temperature. The FT-IR spectra were recorded on a FT-IR spectrophotometer in the range of 4000–400 cm^{-1} (Tensor 27 spectrometer, Bruker, Germany). Sizes based on z-average and Zeta potentials of the NPs were measured by photo-correlation spectroscopy (PCS) (Zetasizer-ZS, Malvern, UK). The morphology and particle size of the NPs was observed and determined using a transmission electron microscopy (LEO960, Denmark). Sample was prepared by dropping the suspension on a carbon-coated copper grid and then drying in vacuum. SEM image of the NPs was captured by SEM-TESCAN MIRA3-FEG. Thermal gravimetric analysis (TGA) was carried out (TGA/SDTA 851/Mettlear Toledo, Spain) by heating rate of 10 °C min^{-1} from 50 to 800 °C under a nitrogen flow. The LCST behavior of samples was determined using a UV–Vis spectrophotometer (Cary-100 UV–Vis, USA). The change in transmittance as a function of temperature was recorded using a 600 nm wavelength. X-ray diffraction (XRD) patterns of all the synthesized materials were detailed using an X-ray diffractometer (D5000, Siemens, Germany) with Cu Kα radiation at 40 kV in the range of 2θ from 20° to 80° and scan rate of 3° min^{-1}. A vibrating-sample magnetometer (VSM; AGFM, Iran) was used to study the magnetic properties of the synthesized magnetic NPs at room temperature. Drug determination was performed on a reversed-phase HPLC system (Knauer, Germany) equipped with a model 1000 HPLC pump and a UV detector model 2600 for measurement of drug. Separation was achieved on a C-18 column (5 μm, 250 × 4.6 mm) (Knauer, Germany) at room temperature.

Results and discussion

Preparation and characterization of polymer@Au/Fe_3O_4 NPs

The polymer@Au/Fe_3O_4 NPs were prepared by 3 sequential steps as shown in Fig. 1. The copolymer containing of thiol side groups was first synthesized by a free-radical polymerization of NIPAAm with IA. Then, AE–S–S–Py was attached covalently to activated carboxylic acids of IA under the formation of amide bonds.

The freeze-dried thiolated polymer had the evidence of a white odorless powder. After the synthesis of thiolated poly(NIPAAm-co-IA), core/shell of Au/Fe_3O_4 was fabricated by reducing $HAuCl_4$ in the presence of Fe_3O_4 by sodium citrate. The citrate stabilized Au/Fe_3O_4 NPs that were grafted through ligand exchange with thiolated polymer, could be received in the one-step process by adding polymer into an Au/Fe_3O_4 aqueous solution. A deep red solution was obtained containing polymer@Au/Fe_3O_4 NPs with a mean diameter of 58.7 nm verified by PCS. Particle size is an important parameter effect in vivo performance and pharmacokinetics of polymeric NPs (Lee et al. 2010). In our research, PCS measurements showed that the mean hydrodynamic diameters of Au/Fe_3O_4 and polymer-coated Au/Fe_3O_4 NPs were 39.6 and 58.7 nm, respectively (Fig. 2a, b). In the measurement of zeta potential, after coating polymer to the Au/Fe_3O_4 NPs, zeta potential value is decreased from −39 to −31 mV, which is only slightly less negative than the uncoated Au/Fe_3O_4 NPs. Although the derivatization of citrate groups of Au led to charge reduction of NPs, the negative charge densities generated by the remaining citrate groups and additional carboxylate groups on the backbone of derivatized copolymer provide enough negative charges to guarantee the colloidal stability of NPs. It was reported that charge density above ±30 mV leads to stability of colloids (Mohanraj and Chen 2006).

We analyzed the Au/Fe_3O_4 with and without polymer coating by PCS and UV–Vis spectroscopy to evaluate the effect of polymer decoration on the size of core NPs. As shown in Fig. 3, the characteristic surface plasmon absorbance (SPA) bond of Au/Fe_3O_4 NPs is observed in the spectrum at approximate 522 nm. After coating of polymer, the UV–Vis spectra

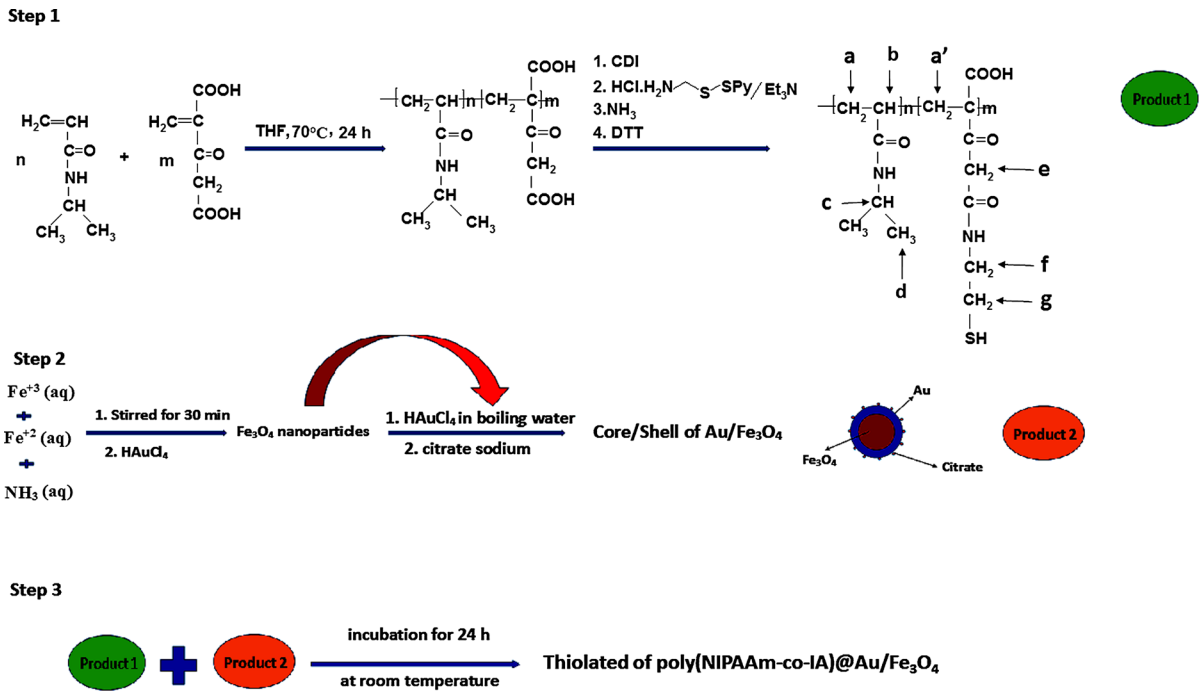

Fig. 1 Schematic illustration for the dual-responsive thiolated poly(NIPAAm-co-IA)@Au/Fe_3O_4 nanoparticles

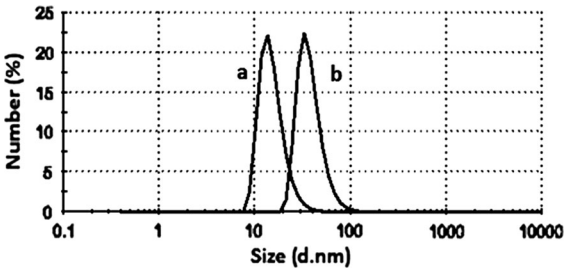

Fig. 2 Size distribution of *a* Au/Fe_3O_4 and *b* polymer@Au/Fe_3O_4 nanoparticles

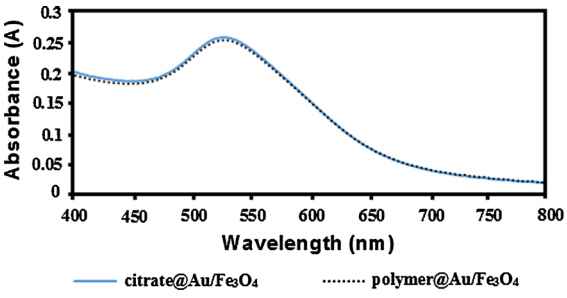

Fig. 3 UV–Vis spectra of citrate@Au/Fe3O4 NPs and polymer@Au/Fe_3O_4 nanoparticles

of the NPs in solution revealed a slight red shift (525) attributed to polymer grafting rather than the agglomeration (Cui 2005a; Zhang et al. 2013).

In order to further study, the shape of polymer-coated Au/Fe_3O_4 NPs was explored by TEM. Figure 4a illustrates a typical TEM image of polymer@Au/Fe_3O_4 NPs in which most of the NPs are spherical in shape with an average diameter of 30 nm confirming the PCS analysis. The NPs are in suitable size range for passive targeted drug delivery to cancerous tissue. It was claimed that the suitable sizes to escape from reticuloendothelial system and infiltrate into leaky cancerous tissues are in the range of 20–100 nm (Cho et al. 2008). The narrow size distribution of prepared NPs was concluded from the PCS analysis results (Fig. 2a). SEM image (Fig. 4b) which shows the large population of particles in the field confirmed the interpretation of PCS pattern.

The presence of NIPAAm and IA monomer in polymer@Au/Fe_3O_4 was also characterized by FT-IR spectra in Fig. 5. The FT-IR spectrum of the polymer exhibited strong absorption peaks at about 1649 cm^{-1} (υ co) and 1544 cm^{-1} (υ_{C-N}) are from the NIPAAm (Fig. 5a). The peak that appeared at 1710 cm^{-1}(υ co) can be ascribed to the C=O stretching vibration of IA

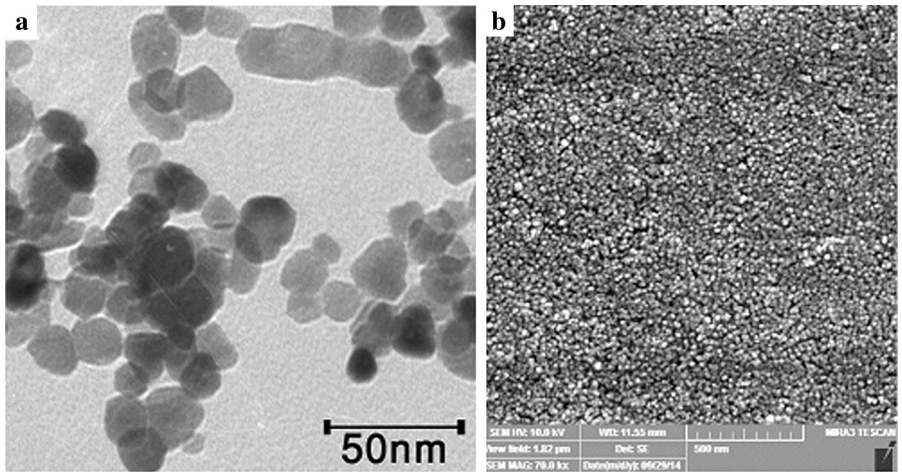

Fig. 4 **a** TEM and **b** SEM images of polymer@Au/Fe_3O_4 nanoparticles

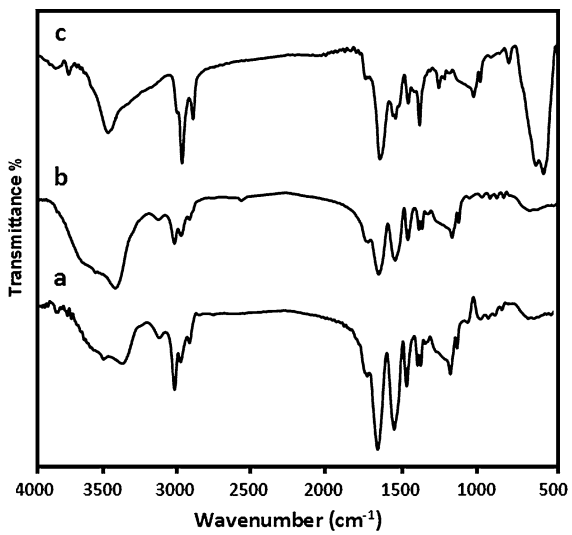

Fig. 5 FTIR spectra of *a* poly(NIPAAm-co-IA) *b* thiolated of poly(NIPAAm-co-IA) *c* polymer@Au/Fe_3O_4 nanoparticles

unit. Furthermore, the stretching vibrations of isopropyl groups of PNIPAAm observed at 1386 and 1370 cm^{-1} and the absorption peak at about 1495 cm^{-1} can be attributed to the $–CH_2$ groups, vicinal to the carbonyl groups of PIA. The spectrum of copolymer containing thiol side groups shows a peak at 2510 cm^{-1} which corresponds to the stretching band of S–H (Shi et al. 2014) (Fig. 5b). In addition, for the polymer@Au–Fe_3O_4 NPs, characteristic peaks of the copolymer that were observed at 1649, 1544, 1710, and the peak at 586 cm^{-1} confirmed the polymer linkage via thiol-Au/Fe_3O_4 bonds (Lo et al. 2007) (Fig. 5c).

The composition of the copolymers containing 13.75 mol% IA in the feeds were characterized by using ^{1}H-NMR spectroscopy (Fig. 6). ^{1}H-NMR spectra were taken in $CDCl_3$. The broad beaks at $\delta = 1.5–1.9$ ppm (a + a′ in Fig. 1) and at $\delta = 2.1–2.5$ ppm (b in Fig. 1) were attributed to the protons of the $–CH_2–$ and $–CH–$ groups in the NIPAAm and IA, respectively. In addition, the proton signals assigned to the isopropyl groups ($–CHMe_2$ at $\delta = 4$ ppm, c and $–CHMe_2$ at $\delta = 1.15$, d in Fig. 1) were observed. The peak at 2.7 ppm (e in Fig. 1) corresponded to CH_2 of IA (attached to carbonyl group), and the short peaks at 2.8 ppm (f in Fig. 1) and

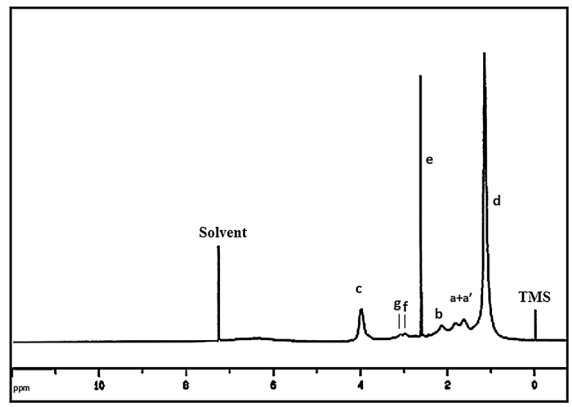

Fig. 6 ^{1}H NMR spectra of thiolated poly(NIPAAm-co-IA) in $CDCl_3$

3.2 ppm (g in Fig. 1) were attributed to the $-CH_2CH_2SH$ and $-CH_2CH_2SH$, respectively (Ossipov et al. 2008). The ratios of the peak areas of signal e to signal d, and the m/n ratio (unit number of NIPAAm/unit number of IA) were estimated to be almost equal to the feed ratios of the two monomers (Fig. 6).

The thermal and pH sensitivities of smart polymer@Au–Fe_3O_4 NPs were probed through monitoring the changes in the optical absorbance of the suspension of the NPs as a function of temperature and pH. The LCST of the NPs was determined with the NP's concentration of 250 mg L^{-1} in PBS (pH 7.4 and 5.3). Optical absorbance of the NPs was measured at 600 nm, and the solution was thermostated for 20 min at stepwise increment of temperature of 1 °C from 20 to 40 °C (Fig. 7). First, we studied the temperature- and pH-responsive behaviors of the polymer@Au–Fe_3O_4 NPs in the distilled water. However, we knew that heating the polymer-coated Au/Fe_3O_4 NPs solution (250 mg L^{-1}) above the LCST of the copolymer did not result in any change in color or opaque of the polymer@Au/Fe_3O_4 (Yusa et al. 2007; Zhang et al. 2013). When the smart polymer-coated Au/Fe_3O_4 NPs were dispersed in PBS with ionic strength of 10 mM, rather than deionized water, the NPs did display temperature-responsive behavior. In this case, the salt effectively screened the surface charge of the dispersed NPs and created a strong aggregation of the functionalized Au/Fe_3O_4 NPs. The effects of salts and ionic strength on the LCST were very important according to the literature (Cui 2005a; Yusa et al. 2007; Zhang et al. 2013). The carboxylic groups of the copolymer induced a pH-dependent LCST behavior of polymer@Au/Fe_3O_4 (Fig. 7). Absorbance of the NP solution decreases with the increasing pH value. With the increasing values of pH, the carboxylic acid groups of IA segment of the copolymer were easily deprotonated resulting in the increase in the hydrophilicity of NPs, and finally leading to an increase in the LCST of the NPs from 37 °C (pH = 5.3) to 40 °C (pH = 7.4).

As shown in Fig. 8, the crystalline nature of the prepared NPs was characterized by XRD analysis. The XRD pattern of Fe_3O_4 NPs showed diffraction peaks at 2θ = 30, 35.63, 43, 54, 57.1, and 62.8 which can be attributed to the (220), (311), (400), (422), (511), and (440) plans of Fe_3O_4 in cubic phase, respectively (Fig. 8a). The diffraction peaks of Au/Fe_3O_4 NPs shown in Fig. 8b depict both Au and Fe_3O_4 NPs, corresponding to Fe_3O_4 (220), (311), (511) and (440); and Au (111), (200), (220), (311), planes. Finally, Fig. 8c displays the presence and the absence of Fe_3O_4 peaks depending on the densities of Au shell and the polymer-coated Au/Fe_3O_4 NPs (Lo et al. 2007).

The magnetization curves indicating the superparamagnetic behaviors of the Fe_3O_4, core/shell Au/Fe_3O_4 NPs and polymer@ Au/Fe_3O_4 NPs measured at room temperature are illustrated at Fig. 9. The saturated magnetization values of Fe_3O_4, Au/Fe_3O_4, and polymer@Au/Fe_3O_4 NPs are 63.2, 29.7, and 18.5 emu g^{-1}, respectively. The reported gradual decrease in the saturated magnetization values by surface modification of core material (Fe_3O_4) can be attributed to a decrease in the magnetic interaction with diamagnetic coating (Zhao et al. 2008). From magnetic studies, it may be inferred that the polymer@Au/Fe_3O_4 NPs show highly desirable superparamagnetic nature for

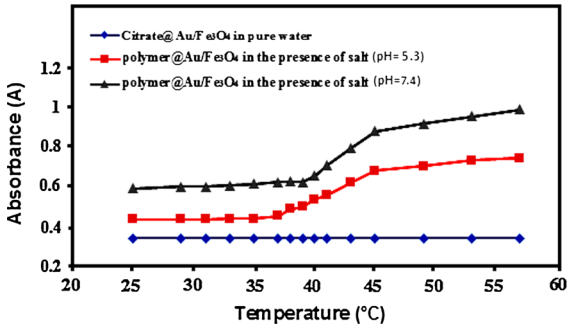

Fig. 7 The temperature- and pH-responsive behaviors of polymer@Au/Fe_3O_4 nanoparticles due to temperature and pH changes. (LCST was probed by absorbance at 600 nm with concentration of 250 mg L^{-1})

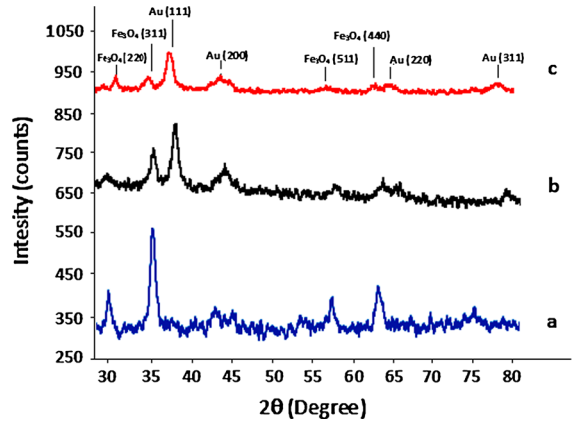

Fig. 8 XRD patterns for *a* Fe_3O_4, *b* Au/Fe_3O_4, and *c* Polymer@Au/Fe_3O_4 nanoparticles

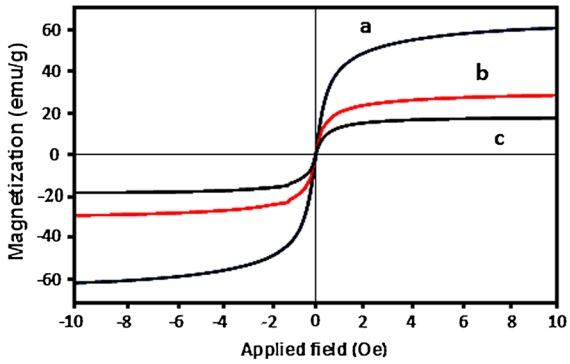

Fig. 9 Magnetization curves of *a* pristine Fe_3O_4, *b* Au/Fe_3O_4, and *c* polymer@Au/Fe_3O_4 nanoparticles at room temperature

magnetic-guided drug delivery applications. Although the magnetic saturation value dropped from 29.7 to 18.5 emu g^{-1} during derivatization of Au/Fe_3O_4 NPs with stimuli-responsive polymer, it is still desired because a magnetization range of 7–22 emu g^{-1} is usually adopted for biomedical applications (Zhang et al. 2014). Figure 10 shows the effect of a permanent magnet on a polymer@Au/Fe_3O_4 NPs solution. The NPs are well dispersed in water when no permanent magnet is placed close to the solution (right image), and all the NPs are concentrated at the left-hand side of the bottle when the magnet is placed close to the solution (left image).

The weight percent of the grafted copolymer layer on the core–shell of Au/Fe_3O_4 NPs was measured by thermogravimetric analysis (TGA). Figure 11 shows two stages of weight loss between 250 °C and 480 °C. The weight loss below 200 °C, corresponds to the loss of water molecules/moisture, which is due to the physically adsorbed water molecules on the surface of polymer@Au/Fe_3O_4 NPs. The massive weight loss between 250 and 350 °C is due to the loss of surface citrate sodium groups, thiol side groups, and decomposition of acidic polymer segments of copolymer. The second weight loss step is from 380 to 500 °C which is due to the degradation of PNIPAAm of copolymer layer. From the percentage weight loss in the TGA curve, the amount of polymer coated on the core/shell of Au/Fe_3O_4 NPs was found to be 44 ± 1 %.

Loading and releasing behaviors of DOX-loaded polymer@Au/Fe_3O_4 NPs

To appraise the capability of the drug adsorption by polymer@Au/Fe_3O_4 NPs as a drug carrier, we used DOX as a model anticancer drug to test the loading and releasing behaviors of DOX. The EE and LC percentages of DOX in polymer@Au/Fe_3O_4 NPs are both found to be 55 % (Since the amount of added drug and polymer are of the same values (5 mg), the calculated EE and LC values—please refer to the text in method

Fig. 10 Digital images of solution of polymer@Au/Fe_3O_4 nanoparticles, dispersion of magnetic nanoparticles, and magnetic response of nanoparticles (*right* to *left*)

Section "Loading of drug in polymer@Au/Fe3O4 NPs"—would be the same). The DOX molecules were easily adsorbed onto the NPs due to the electrostatic interaction between the positively charged DOX molecules and the negatively charged itaconic acid segments of the polymer chain. The cumulative release of DOX is shown in Fig. 12. Drug-release studies of the NPs were performed under physiologic and simulated tumor tissue conditions (PBS, pH 7.4 and 5.3). Under acidic conditions (pH 5.3), the release of DOX was faster than the physiologic condition (pH 7.4) probably due to the decrease in the electrostatic charge of acidic segments of polymer and consequently, to the reduction in its capability for interaction with DOX molecules. The profile of drug release showed effective changes with the temperature variations around the LCST. At 37 °C (below the LCST), only 20 % of loaded drug was released; however, by increasing the temperature to 40 °C, the drug release was faster. The release of higher DOX value (59 %) at 40 °C than normal tissue temperature could be attributed to the collapse of polymeric shell. In other words, by heating to 40 °C (above the LCST), the copolymer aggregates become more hydrophobic. Consequently, the hydrogen bonds between copolymer and water are destroyed, and accordingly, the copolymer aggregates become more aggregated. Therefore, this polymer shell that shrinks at 40 °C facilitates the release of loaded drug from the inside of NPs (Cui et al. 2012; Sahoo et al. 2013). These evidences indicated that the effects of thermo and pH responsive behaviors play the main role in drug-release patterns of developed NPs which make them well-deserved carriers to be administered for effective drug delivery to cancer cells.

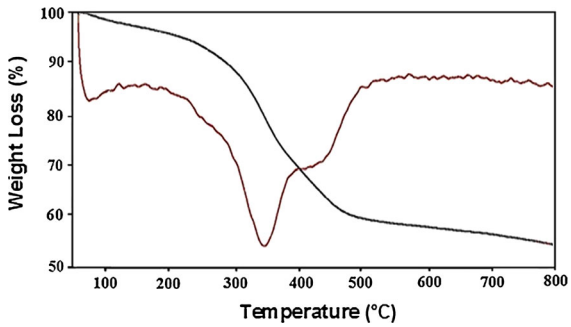

Fig. 11 Thermal analysis curve of polymer@Au/Fe_3O_4 nanoparticles

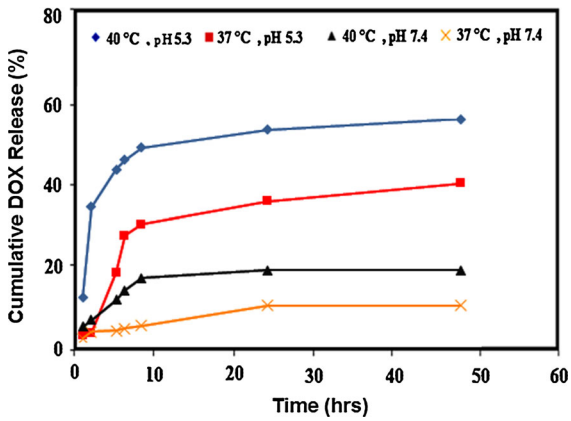

Fig. 12 Cumulative in vitro release profiles of DOX at different conditions from Dox-loaded nanoparticles

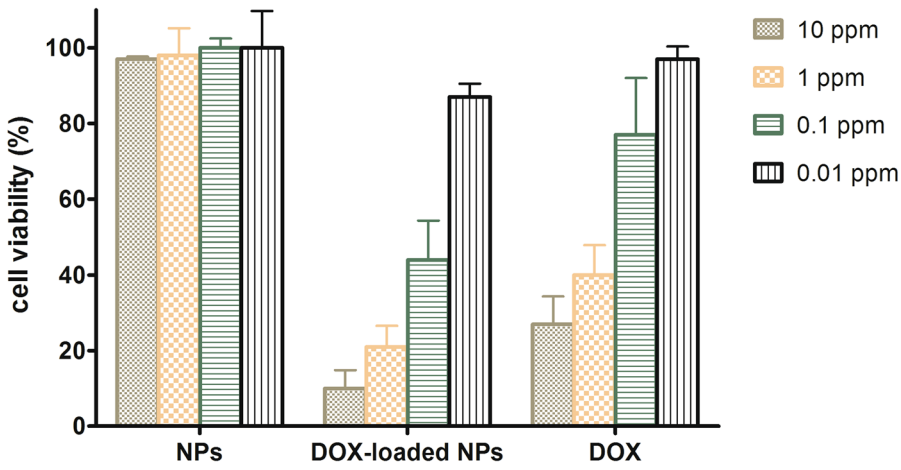

Fig. 13 Cell viability of DOX-free polymer@Au/Fe_3O_4 nanoparticles and DOX-loaded nanoparticles at various concentrations versus A549 cell line for 72 h. (mean ± SD, $n = 5$)

In vitro cytotoxicity

An MTT assay was performed to quantify the cell viability of a lung carcinoma cell line (A549 cells) and investigation of the therapeutic efficacy of DOX-loaded NPs. To evaluate of the cytotoxic effects of DOX-free polymer@Au/Fe_3O_4 NPs and DOX-loaded NPs at four different concentrations, ranging from 0.01 to 10 μg mL^{-1}, were incubated with A549 cells for 72 h. As indicated, the polymer@Au/Fe_3O_4 NPs without DOX exhibited no significant toxicity on A549 cell's viability after 72 h (nearly around 100 % cells are viable after treatment with 10 μg/mL of polymer@Au/Fe_3O_4). Figure 13 compares the cytotoxicity profiles of the DOX, NPs without DOX and DOX-loaded NPs. DOX-loaded NPs showed higher inhibition activity after 72 h in comparison with DOX. Enhanced inhibition of cell growth for DOX-loaded NPs in comparison with free form of drug would be advantageous in lowering the dose of anticancer drug in application. The results showed that the polymer@Au/Fe_3O_4 NPs offer an efficient anticancer dual delivery system. Hence, it can be claimed that the administration dose can be decreased to have the same clinical response when higher amounts of DOX are used.

Conclusion

The smart core/shell of Au/Fe_3O_4 NPs by stimuli-responsive polymeric shell with thiol side groups were newly developed for application as a carrier of well-known potent anticancer agent, DOX. These multi-functional core/shell NPs were created to act as potentially capable thermo and pH-responsive drug delivery carriers, specifically suitable in cancer therapy. TEM image showed the mean size of the NPs to be around ~30 nm which is in the required size-distribution range suitable for passive targeting drug delivery to cancerous tissue. All the obtained results for the size, shape, and size distribution were confirmed by PCS, TEM, and SEM techniques, respectively. The prepared DOX-NPs displayed long-term colloidal stability with superparamagnetic property at room temperature and quite high loading drug indexes (EE, and LC values of 55 %). These smart NPs exhibited pH- and thermoresponsive DOX-release characteristics in PBS. It was concluded that our developed NPs may throw open the possibilities for the targeted delivery of DOX to the cancerous tissues.

Acknowledgments The authors acknowledge the financial support from the University of Tabriz.

References

Bawa P, Pillay V, Choonara YE, Toit LC (2009) Stimuli-responsive polymers and their applications in drug delivery. Biomed Mater 4:1–15. doi:10.1088/1748-6041/4/2/022001

Chao X, Shi F, Zhao YY, Li K, Peng M, Chen C, Cui YL (2010) Cytotoxicity of Fe_3O_4/Au composite nanoparticles loaded with doxorubicin combined with magnetic field. Pharmazie 65:500–504. doi:10.1691/ph.2010.9362

Chao X, Guo L, Zhao Y, Hua K, Peng M, Chen C, Cui Y (2011) PEG-modified GoldMag nanoparticles (PGMNs) combined with the magnetic field for local drug delivery. J Drug Target 19:161–170. doi:10.3109/10611861003801842

Cho K, Wang X, Nie S, Chen Z, Shin DM (2008) Therapeutic nanoparticles for drug delivery in cancer. Clin Cancer Res 14:1310–1316. doi:10.1158/1078-0432.CCR-07-1441

Cui Y, Hui W, Su J, Wang Y, Chen C (2005a) Fe_3O_4/Au composite nano-particles and their optical properties. Sci China, Ser B 48:273–278. doi:10.1360/042004-51

Cui Y, Wang Y, Hui W, Zhang Z, Xin X, Chen C (2005b) The synthesis of GoldMag nano-particles and their application for antibody immobilization. Biomed Microdevices 7:153–156. doi:10.1007/s10544-005-1596-x

Cui W, Lu X, Cui K, Niu L, Wei Y, Lu Q (2012) Dual-responsive controlled drug delivery based on ionically assembled nanoparticles. Langmuir 28:9413–9420. doi:10.1021/la3016436

Du B, Mei A, Tao P, Zhao B, Cao Z, Nie J, Xu J, Fan Z (2009) Poly[N -isopropylacrylamide- co -3-(trimethoxysilyl)-propylmethacrylate] coated aqueous dispersed thermosensitive Fe_3O_4 nanoparticles. J Phys Chem C 113:10090–10096. doi:10.1021/jp9016536

Dykman L, Khlebtsov N (2012) Gold nanoparticles in biomedical applications: recent advances and perspectives. Chem Soc Rev 41:2256–2282. doi:10.1039/c1cs15166e

Ebright YW, Chen Y, Pendergrast PS, Ebright RH (1992) Incorporation of an EDTA-metal complex at a rationally selected site within a protein: application to EDTA-iron DNA affinity cleaving with catabolite gene activator protein (CAP) and Cro. Biochemistry 31:10664–10670. doi:10.1021/bi00159a004

Ganta S, Devalapally H, Shahiwala A, Amiji M (2008) A review of stimuli-responsive nanocarriers for drug and gene delivery. J Control Release 126:187–204. doi:10.1016/j.jconrel.2007.12.017

Hamner KL, Maye MM (2013) Thermal aggregation properties of nanoparticles modified with temperature sensitive copolymers. Langmuir 29:15217–15223. doi:10.1021/la4037887

Hamner KL, Alexander CM, Coopersmith K, Reishofer D, Provenza C, Maye MM (2013) Using temperature-

sensitive smart polymers to regulate DNA-mediated nanoassembly and encoded nanocarrier drug release. ACS Nano 7:7011–7020. doi:10.1021/nn402214e

Kast CE, Bernkop-Schnürch A (2002) Polymer–cysteamine conjugates: new mucoadhesive excipients for drug delivery? Int J Pharm 234:91–99. doi:10.1016/S0378-5173(01)00955-3

Lee H, Fonge H, Hoang B, Reilly RM, Allen C (2010) The effects of particle size and molecular targeting on the intratumoral and subcellular distribution of polymeric nanoparticles. Mol Pharm 7:1195–1208. doi:10.1021/mp100038h

Li C, Chen T, Ocsoy I, Zhuet C, Yasun E, You M, Wu C, Zheng J, Song E, Huang CZ, Tan W (2014a) Gold-Coated Fe_3O_4 nanoroses with five unique functions for cancer cell targeting, imaging and therapy. Adv Funct Mater 24:1772–1780. doi:10.1002/adfm.201301659

Li J, Wu W, Han C, Zhang S, Zhou H, Guo J (2014b) Aggregation behavior of pH- and thermo-responsive block copolymer protected gold nanoparticles. Colloid Polym Sci 292:1657–1664. doi:10.1007/s00396-014-3225-9

Liang Z, Wu X, Xie Y, Liu S (2012) A facile Approach to fabricate water-soluble Au–Fe_3O_4 nanoparticle for liver cancer cells imaging. Chin J Chem 30:1387–1392. doi:10.1002/cjoc.201100692

Lin JJ, Chen JS, Huang SJ, Ko JH, Wang YM, Chen TL, LiF Wang (2009) Folic acid-Pluronic F127 magnetic nanoparticle clusters for combined targeting, diagnosis, and therapy applications. Biomaterials 30:5114–5124. doi:10.1016/j.biomaterials.2009.06.004

Liu TY, Hu SH, Liu TY, Liu DM, Chen SY (2006) Magnetic-sensitive behavior of intelligent ferrogels for controlled release of drug. Langmuir 22:5974–5978. doi:10.1021/la060371e

Liu H, Hou P, Zhang W, Kim YK, Wu JH (2010) The synthesis and characterization of polymer-coated FeAu multifunctional nanoparticles. Nanotechnology 21:1–9. doi:10.1088/0957-4484/21/33/335602

Liu J, Huang Y, Kumar A, Tan A, Jin S, Mozhi A, Liang X-J et al (2014) pH-sensitive nano-systems for drug delivery in cancer therapy. Biotechnol Adv 32:693–710. doi:10.1016/j.biotechadv.2013.11.009

Lo CK, Xiao D, Choi MMF (2007) Homocysteine-protected gold-coated magnetic nanoparticles: synthesis and characterisation. J Mater Chem 17:2418–2427. doi:10.1039/b617500g

Lowe AB, Sumerlin BS, Donovan MS, McCormick CL (2002) Facile preparation of transition metal nanoparticles stabilized by well-defined (co)polymers synthesized via aqueous reversible addition-fragmentation chain transfer polymerization. J Am Chem Soc 124:11562–11563. doi:10.1021/ja020556h

Mahmoudi M, Sant S, Wang B, Laurent S, Senf T (2011) Superparamagnetic iron oxide nanoparticles (SPIONs): development, surface modification and applications in chemotherapy. Adv Drug Deliv Rev 63:24–46. doi:10.1016/j.addr.2010.05.006

Massart R (1981) Preparation of aqueous magnetic liquids in alkaline and acidic media. IEEE Trans Magn 17:1247–1248. doi:10.1109/TMAG.1981.1061188

Mohanraj VJ, Chen Y (2006) Nanoparticles—A review. Trop J Pharm Res 5:561–573. doi:10.4314/tjpr.v5i1.14634

Nigam S, Chandra S, Newgreen DF, Bahadur D, Chen Q (2014) Poly(ethylene glycol)-modified PAMAM-Fe_3O_4-doxorubicin triads with the potential for improved therapeutic efficacy: generation-dependent increased drug loading and retention at neutral pH and increased release at acidic pH. Langmuir 30:1004–1011. doi:10.1021/la404246h

Nuopponen M, Tenhu H (2007) Gold nanoparticles protected with pH and temperature-sensitive diblock copolymers. Langmuir 23:5352–5357. doi:10.1021/la063240m

Ossipov D, Piskounova S, Hilborn J (2008) Poly (vinyl alcohol) cross-linkers for in vivo injectable hydrogels. Macromolecules 41:3971–3982. doi:10.1021/ma800332c

Sahoo B, Devi KSP, Banerjee R, Maiti TK, Pramanik P, Dhara D (2013) Thermal and pH responsive polymer-tethered multifunctional magnetic nanoparticles for targeted delivery of anticancer drug. ACS Appl Mater Interfaces 5:3884–3893. doi:10.1021/am400572b

Salehi R, Hamishehkar H (2014) Development of dual responsive nanocomposite for simultaneous delivery of anticancer drugs. J Drug Target 22:327–342. doi:10.3109/1061186X.2013.876645

Salehizadeh H, Hekmatian E, Sadeghi M, Kennedy K (2012) Synthesis and characterization of core-shell Fe_3O_4-gold-chitosan nanostructure. J Nanobiotechnol 10:1–7. doi:10.1186/1477-3155-10-3

Salmaso S, Caliceti P, Amendola V, Meneghetti M, Magnusson JP, Pasparakis G, Alexander C (2009) Cell up-take control of gold nanoparticles functionalized with a thermoresponsive polymer. J Mater Chem 19:1608–1615. doi:10.1039/b816603j

Shi F, Hui W, Cui Y, Chen C (2011) Surface modification and characterization of Fe_3O_4/Au composite nanoparticles. Nano 6:145–151. doi:10.1142/S1793292011002469

Shi S, Wang Q, Wang T, Ren S, Gao Y, Wang N (2014) Thermo-, pH-, and light-responsive poly(*N*-isopropylacrylamide-co-methacrylic acid)–Au hybrid microgels prepared by the in situ reduction method based on Au-thiol chemistry. J Phys Chem B 118:7177–7186. doi:10.1021/jp5027477

Siegel RA (2014) Stimuli sensitive polymers and self regulated drug delivery systems: a very partial review. J Control Release 190:337–351. doi:10.1016/j.jconrel.2014.06.035

Sundaresan V, Menon JU, Rahimi M, Nguyen KT, Wadajkar AS (2014) Dual-responsive polymer-coated iron oxide nanoparticles for drug delivery and imaging applications. Int J Pharm 466:1–7. doi:10.1016/j.ijpharm.2014.03.016

Tamer U, Gündoğdu Y, Boyacı İH, Pekmez K (2009) Synthesis of magnetic core–shell Fe_3O_4–Au nanoparticle for biomolecule immobilization and detection. J Nanoparticle Res 12:1187–1196. doi:10.1007/s11051-009-9749-0

Yang HM, Park CW, Bae PK, Ahn T, Seo BK, Chung BH, Kim J-D (2013) Folate-conjugated cross-linked magnetic nanoparticles as potential magnetic resonance probes for in vivo cancer imaging. J Mater Chem B 1:3035–3043. doi:10.1039/c3tb20295j

Yusa S, Fukuda K, Yamamoto T, Iwasaki Y, Watanabe A, Akiyoshi K, Morishima Y (2007) Salt effect on the heat-induced association behavior of gold nanoparticles coated with poly(*N*-isopropylacrylamide) prepared via reversible addition-fragmentation chain transfer (RAFT) radical polymerization. Langmuir 23:12842–12848. doi:10.1021/la702741q

Zhang Z, Maji S, da Antunes ABF, Rycke RD, Zhang Q, Hoogenboom R, de Geest BG (2013) Salt plays a pivotal role in the temperature-responsive aggregation and layer-by-layer assembly of polymer-decorated gold nanoparticles. Chem Mater 25:4297–4303. doi:10.1021/cm402414u

Zhang W, Deng L, Wang G, Guo X, Li Q, Zhang J, Khashab NM (2014) Low-magnetization magnetic microcapsules: a synergistic theranostic platform for remote cancer cells therapy and imaging. Part Part Syst Charact 31:985–993. doi:10.1002/ppsc.201400005

Zhao X, Cai Y, Wang T, Shi Y, Jiang G (2008) Preparation of alkanethiolate-functionalized core/shell Fe_3O_4@Au nanoparticles and its interaction with several typical target molecules. Anal Chem 80:9091–9096. doi:10.1021/ac801581m

Zhao Z, Huang D, Yin Z, Chi X, Wang X, Gao J (2012) Magnetite nanoparticles as smart carriers to manipulate the cytotoxicity of anticancer drugs: magnetic control and pH-responsive release. J Mater Chem 22:15717–15725. doi:10.1039/c2jm31692g

Zheng P, Jiang X, Zhang X, Zhang W, Shi L (2006) Formation of gold@polymer core-shell particles and gold particle clusters on a template of thermoresponsive and pH-responsive coordination triblock copolymer. Langmuir 22:9393–9396. doi:10.1021/la0609064

Zhu Y-J, Chen F (2015) pH-Responsive drug-delivery systems. Chem—An Asian J 10:284–305. doi:10.1002/asia.201402715